The Extended Interactions and Gla Domain of Blood Coagulation Factor Xa†

Stephanie X. Wang,[‡,§] Eugene Hur,[§,||] Carolyn A. Sousa,[⊥] Linda Brinen,[⊥] Eric J. Slivka,[||] and Robert J. Fletterick*[,⊥]

Graduate Program in Chemistry and Chemical Biology, Graduate Group in Biophysics, and Departments of Biochemistry and Biophysics, University of California, San Francisco, California 94143

Received December 9, 2002; Revised Manuscript Received April 11, 2003

ABSTRACT: The serine protease factor Xa (FXa) is inhibited by ecotin with picomolar affinity. The structure of the tetrameric complex of ecotin variant M84R (M84R) with FXa has been determined to 2.8 Å. Substrate directed induced fit of the binding interactions at the S2 and S4 pockets modulates the discrimination of the protease. Specifically, the Tyr at position 99 of FXa changes its conformation with respect to incoming ligand, changing the size of the S2 and S4 pockets. The role of residue 192 in substrate and inhibitor recognition is also examined. Gln 192 from FXa forms a hydrogen bond with the P2 carbonyl group of ecotin. This confirms previous biochemical and structural analyses on thrombin and activated protein C, which suggested that residue 192 may play a more general role in mediating the interactions between coagulation proteases and their inhibitors. The structure of ecotin M84R−FXa (M84R−FXa) also reveals the structure of the Gla domain in the presence of Mg^{2+}. The first 11 residues of the domain assume a novel conformation and likely represent an intermediate folding state of the domain.

Blood vessel trauma initiates a proteolytic cascade of serine proteases that culminates in the cross-linking of the clotting protein fibrin and the formation of blood clots. The coagulation cascade is composed of two interconnected pathways: the extrinsic and the intrinsic, which converge in the activation of zymogen factor X (FX) to functional factor Xa (FXa). This activation occurs either by the factor VIIa (FVIIa)-tissue factor complex (extrinsic pathway) or by the factor IXa (FIXa)-factor VIII complex (intrinsic pathway). Mature FXa consists of two disulfide linked polypeptide chains: a light chain composed of an N-terminal γ-carboxyglutamate (Gla) containing Gla domain, followed by two epidermal-growth-factor-like (EGF) domains, and a heavy chain harboring a trypsin-like serine protease domain (*1*, *2*). In the presence of its cofactor, factor Va (FVa), FXa cleaves the zymogen prothrombin to generate active thrombin protease.

Because of its dual role as both the final enzyme of the cascade and a positive feedback regulator of the intrinsic pathway, thrombin has historically been the major protease target of the blood coagulation cascade in the development of anti-coagulant therapies. However, because thrombin is so ubiquitous in the blood coagulation response, many thrombin inhibitors have had low safety to efficacy profiles in clinical trials, with their usage often associated with an increased risk of bleeding complications (*3*).

The search for alternative targets has led to FXa. Like thrombin, it is strategically placed to regulate both the intrinsic and the extrinsic pathways, but because of its more restricted activity, it is thought that inhibiting the upstream FXa would be more efficient and less likely to elicit the side effects seen with thrombin inhibitors. However, similarities of structure and substrate selection among the serine proteases of the blood coagulation cascade have challenged the design of specific inhibitors against FXa (*1*, *4*). Interactions between FXa and its inhibitors have not been investigated as thoroughly as interactions between thrombin and its inhibitors. X-ray crystallography has been used to define several FXa−inhibitor complexes (*2*, *5*−*9*). However, no structure of FXa with a canonically bound macromolecular inhibitor showing the substrate-like interactions at both sides of the scissile bond has been determined. Because of the importance of extended interactions in FXa substrate specificity (*10*), such a complex may prove to be especially useful in inhibitor design.

The *Escherichia coli* macromolecular protease inhibitor ecotin (*11*) inhibits a broad range of serine proteases of the chymotrypsin fold including trypsin, chymotrypsin, and collagenase (*12*, *13*). Previous structural analyses showed that inhibition by ecotin occurs by the formation of a tetrameric complex consisting of a domain swapped ecotin dimer binding two protease molecules (*14*−*17*). Each ecotin molecule binds its target at two distinct sites on the protease: a primary site and a secondary site. The primary site interaction is characterized by substrate-like binding of the 80's loop of ecotin to the active site cleft of the protease. Binding at the secondary site involves less specific interactions involving the distally located 60's loop of ecotin with a flat, hydrophobic patch on the protease.

† This work was supported by the UC Biotechnology STAR Project.

* Corresponding author. E-mail: flett@msg.ucsf.edu. Phone: (415) 476-5080. Fax: (415) 476-1902.

‡ Graduate Program in Chemistry and Chemical Biology, currently in the Department of Pathology.

§ These authors contributed equally to this work.

|| Graduate Group in Biophysics.

⊥ Departments of Biochemistry and Biophysics.

10.1021/bi027320a CCC: $25.00
Published on Web 06/10/2003

Ecotin is the most potent reversible inhibitor of FXa, with an inhibition constant (K_i) of 54 pM (*12*). An M84R mutation of the P1 residue of ecotin further increases inhibition by 5-fold to 11 pM (*12*). We have crystallized and determined the X-ray structure of human FXa in complex with ecotin M84R (M84R). The canonical binding mode of the ecotin 80's loop provides valuable insights into the role of extended interactions in FXa substrate recognition. Comparisons with the existing structure of thrombin-M84R reveal how ecotin adapts to different proteases to achieve high affinity binding (*17*).

The structure of FXa-ecotin M84R (M84R−FXa) is also the first structure of FXa determined in the presence of an ordered Gla domain. The Gla domain is a highly conserved N-terminal domain found in many of the proteins involved in blood coagulation including factors VII, IX, and X; proteins C, S, and Z; and prothrombin. About 45 amino acids in length, the Gla domain is characterized by 9 to 12 γ-carboxyglutamates that are added post-translationally by a vitamin K-dependent carboxylase (*18*). In the presence of Ca^{2+}, the Gla domain binds negatively charged phospholipids, anchoring the protein to the membrane surface. This is thought to be critical for the proper functioning of these proteins, as binding to the membrane not only assists in localizing these enzymes to sites of injury but also helps properly position them for interaction with activators, cofactors, and substrates (*1*).

Previously, the Gla domain of FXa was either disordered or proteolytically cleaved from full-length FXa to aid in crystallization (*2*, *5*−*9*, *19*). The Gla domain of M84R−FXa, however, was well ordered. This represents the first structure in the presence of an ordered Gla domain as well as the first crystal structure of the Gla domain in the presence of Mg^{2+}. Three bound Mg^{2+} ions define the locations of three high affinity, low specificity cation binding sites predicted in earlier studies (*20*−*23*). The structure thus provides a glimpse of an intermediate folding state of the domain and provides key insights into how the Gla domain attains the membrane bound state.

MATERIALS AND METHODS

Purification and Crystallization of the FXa−Ecotin M84R Complex. Ecotin M84R was purified by standard procedures as described (*24*, *25*) and subsequently sent to Haematologic Technologies Inc. (Essex Junction, VT) to be complexed with purified FXa from human plasma. Equimolar quantities of FXa and ecotin M84R were incubated on ice before being purified by gel filtration in the presence of 150 mM NaCl, 2 mM $MgCl_2$, and 20 mM Tris at pH 7.4.

The purified M84R−FXa complex was concentrated to 5.4 mg/mL and crystallized at room temperature by the sitting drop method. Initial crystals were obtained by the PEG/Ion screen (Hampton Research) with a well solution containing 20% PEG 3350 and 0.2 M sodium potassium tartrate at pH 7.1. Final crystals were optimized by adding a trace amount of glycerol (to a final concentration of 2%) and 1 μL of MPD to 4 μL of well solution and 5 μL of protein solution.

Data Collection, Structure Determination, and Refinement. Orthorhombic crystals of M84R−FXa diffracted to 2.8 Å. A full data set was collected at the Advanced Light Source (ALS) beamline 5.0.2 with an ADSC Quantum 4 CCD detector. Data sets were integrated and merged using SCALEPACK/DENZO (*26*). The symmetry of crystals of M84R−FXa is described by the space group *I*222, with a = 66.8 Å, b = 108.0 Å, and c = 186.3 Å. Data statistics indicated that one FXa and one ecotin molecule were present per asymmetric unit. Solvent content was estimated to be 58%.

Table 1: Data and Refinement Statistics for Ecotin M84R−FXa Complex

structure	M84R−FXa
space group	*I*222
unit cell constants (Å)	
a	66.8
b	108.0
c	186.3
highest resolution (Å)	2.8
unique reflections	16994
completeness	92.9%
$\langle I/I_\sigma \rangle$	11.2
R_{merge}[a]	9.3% (three data sets)
solvent content	57.6%
R[b]after molecular replacement	41%
refinement resolution range (Å)	20.0−2.8
R	20.7%
free R[c]	23.4%
water molecules	51
rmsd in bond lengths (Å)	0.008
rmsd in bond angles (deg)	1.4

[a] $R_{merge} = \sum|(I - \langle I \rangle)|/\sum(I)$. [b] $R = \sum_{hkl}(|F_{obs}(hkl)| - k|F_{calc}(hkl)|)^2/\sum_{hkl}|F_{obs}(hkl)|$. [c] Free R: cross-validation R calculated by omitting 10% of the reflections (*61*).

The structure of M84R−FXa was solved using molecular replacement with rotation and translation functions from CNS 1.0 (*27*). Data to 3.5 Å were used in all rotation searches. Initially, a heterodimer search model of FXa (from PDB 1FAX) bound to ecotin (from PDB 1ID5) was constructed based on the structure of trypsin−ecotin (*14*) using Insight II (Accelrys, San Diego, CA). The light chain of FXa was omitted in this model for molecular replacement. This heterodimer model, however, did not result in any rotation solutions that could be improved by further translation searches. A second approach was undertaken involving a two step rotation search. Rotation solutions from a first search using the heavy chain of FXa were used to fix the orientation of FXa in a second search using ecotin as the search model. The top 10 solutions from the second rotation search were then subjected to translation searches and rigid body refinement using data to 2.8 Å to produce a starting model of M84R−FXa with an initial R value of 43.5%. The final structure was refined to 2.8 Å with an R of 20.7% and an R_{free} of 23.4% using CNS 1.0/1.1 (*27*) and Quanta 2000 (Molecular Simulations Inc., San Diego CA). Detailed data and refinement statistics are listed in Table 1. The coordinates of M84R−FXa have been deposited in the Protein Data Bank under accession code 1P0S.

Buried surface areas between protein domains were calculated by the program NACCESS (*28*). Superposition data were calculated with LSQMAN (*29*). The relative orientations between superimposed molecules were calculated by the program GEM (*30*). Figure 1 was made with Molscript and Raster3D (*31*). Figure 2B was generated with Ligplot (*32*). All other figures were made with Pymol (*33*).

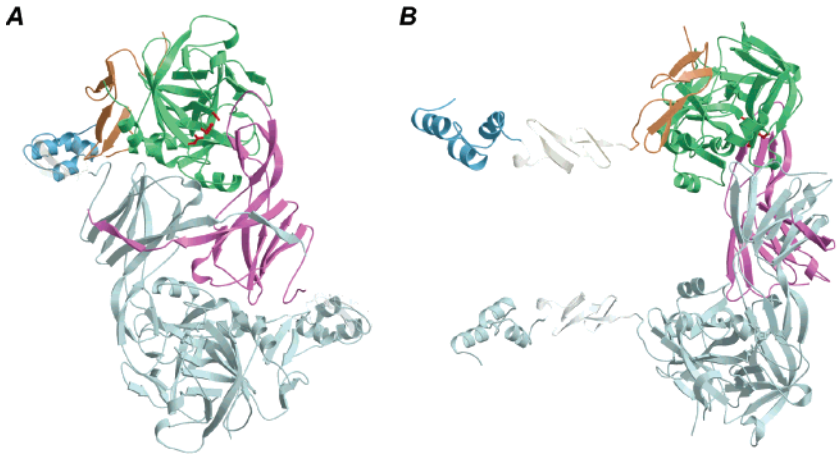

FIGURE 1: Ribbon diagram of the tetrameric FXa-ecotin M84R complex. Panel A is rotated 90° with respect to panel B. The Gla domain is shown in blue; the EGF2 domain in orange; the catalytic domain in green; and ecotin M84R in purple. The catalytic triad is shown in red. The EGF1 domain (transparent white) was disordered and modeled using the EGF1 domain from PDB 1XKA. The symmetry mate that comprises the other half of the tetrameric complex is shown in gray.

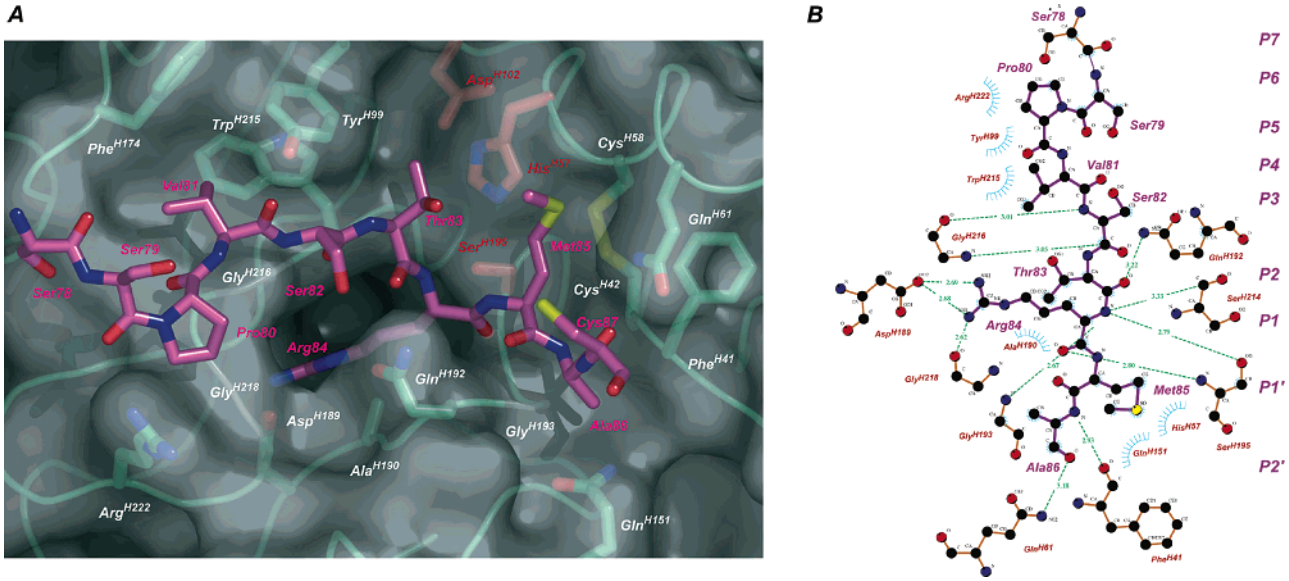

FIGURE 2: Extended interactions between FXa and ecotin M84R shown in panel A as a three-dimensional surface rendering of FXa, with ecotin residues 78−86 in purple, FXa in green, and the catalytic triad highlighted in red and in panel B as a two-dimensional Ligplot (*32*).

RESULTS AND DISCUSSION

Overall Structural Features of the FXa−Ecotin M84R Complex. Like other ecotin−protease complexes, ecotin M84R binds as a dimer to two FXa molecules, forming a tetramer via two distinct binding sites on the protease: a primary site at the active site and a secondary site located distally near the C-terminus (Figure 1A). Both binding interactions occur on the heavy chain of FXa. The light chain of FXa binds to the heavy chain via the C-terminal EGF domain (EGF2) in an extended conformation that is nearly perpendicular to the complex formed between the heavy chain and ecotin (Figure 1B). The Gla domain is involved in crystal contacts primarily with the heavy chain of a neighboring symmetry mate. Surprisingly, the N-terminal EGF domain (EGF1) was found to be disordered. Numerous sparse density peaks in this region were observed in electron density maps, but efforts to trace a backbone through these peaks did not improve refinement statistics or result in improved density. The EGF1 domain was therefore omitted from the model.

Overall, M84R−FXa maintains the general tetrameric features found in other ecotin−protease complexes. However, comparisons of M84R−FXa with the structure of thrombin−ecotin M84R reveal that the relative orientation between ecotin and protease, as measured by the major angle between the major axis of the two proteins, differs by nearly 8°.

Extended Interactions between Ecotin M84R and FXa. It was previously thought that the specificity of FXa relied mostly on the P1[1] Arg residue, making FXa more similar to the digestive protease trypsin than thrombin. However, when the reactive site loop of the serpin antithrombin (AT) was replaced by the two corresponding P4′−P4 fragments from the FXa cleavage sites in prothrombin, its capacity in inactivating FXa was significantly altered (*10*). This observa-

[1] Protease−ligand interaction is described by conventional nomenclature. Residues in the substrate are labeled $^{+}NH_3$-...P4-P3-P2-P1-P1′-P2′-P3′-P4′...-COO^{-}. The P1−P1′ peptide bond is cleaved by the protease. The corresponding subsites on the enzyme are labeled ...S4-S3-S2-Sl-S1′-S2′-S3′-S4′...(*34*) so that the P2 residue of the ligand binds in the S2 pocket of the enzyme. Pockets N- and C-terminal to the cleaved bond constitute the nonprimed and primed sites, respectively.

tion suggested a significant role for extended interactions in FXa substrate recognition whose details small molecule inhibitors may not have revealed. Because ecotin is not hydrolyzed when bound to FXa, it was possible to observe interactions between FXa and inhibitor on both sides of the scissile bond. The entire buried surface area of interactions between the primary site of ecotin and FXa is 1980 Å^2. Detailed interactions, spanning from ecotin residue 78−86, are depicted in Figure 2A,B.

Like most serine proteases from the blood coagulation cascade, FXa prefers substrates with an Arg at the P1 site. In the M84R−FXa structure, the positively charged side chain of Arg84 of ecotin forms two salt bridges with the negatively charged side chain of Asp^{H189}, as well as a hydrogen bond with the carbonyl oxygen of Gly^{H218} (to distinguish FXa from ecotin residues, FXa residue numbers are written as superscript following its chain label: H for heavy chain and L for light chain). The aliphatic part of the Arg side chain is sandwiched between two groups of hydrophobic residues, with the first group formed by Ala^{H190}, Cys^{H191}, and Cys^{H220} and the second group formed by Val^{H213} and Tyr^{H228}. The main chain atoms of P1 Arg are coordinated by four hydrogen bonds from three protease residues: Gly^{H193}, Ser^{H195}, and Ser^{H214} (Figure 2A,B).

It is interesting to note that while an M84R mutation in ecotin increases the binding affinity for thrombin by over 10^4-fold (*17*), the same mutation increases the binding affinity for FXa by only 5-fold (*12*). This apparent discrepancy can be explained by the presence of a bulky 60's loop insertion in thrombin. By obstructing access to the active site cleft, this loop hinders the establishment of the full array of interactions necessary for binding. Tighter binding to the S1 pocket caused by an M84R mutation provides energy to displace the 60's loop and ensure the proper register of interactions between the 80's loop of ecotin and the residues of the thrombin active site cleft (*17*). Thus, in the case of thrombin, the observed increase in inhibition upon an ecotin M84R mutation is not solely attributable to the energetic contribution of a single Arg side chain. In contrast, the absence of a protruding 60's loop in FXa results in a more open active site. This allows the 80's loop of ecotin to establish the full extent of interactions with FXa without having to overcome an energy barrier caused by the displacement of an obstructing surface loop. As a result, the interactions of both wild-type and M84R ecotin with FXa are very similar, resulting in a far less dramatic change in inhibition constants.

The M84R−FXa structure reveals that the hydrophobic S2 pocket is defined by residues His^{H57}, Tyr^{H60}, Phe^{H94}, Tyr^{H99}, and Ser^{H214} (Figure 2A,B). Previous modeling suggested that larger hydrophobic residues would bind well in the S2 pocket. This was confirmed by in vitro substrate scanning analyses that showed Gly, the highly conserved natural P2 residue, was only slightly better, or in some cases, even worse than the much bulkier residues of Trp, Phe, or Tyr (*35*, *36*). Although existing FXa−inhibitor structures and known natural substrates of FXa argue for a small and shallow S2 pocket, the M84R−FXa structure reveals an unusual conformation of Tyr^{H99} that explains the apparent paradox for the S2 pocket size (Figure 3A). In M84R−FXa, Tyr^{H99} swings 70° away from the P2 Thr, dramatically increasing the size of the S2 pocket. This unusual conformation of Tyr^{H99} is firmly held by two hydrogen bonds between the terminal O_η from Tyr^{H99} and the carbonyl oxygens from ecotin residues Leu52 and Val81. It is clear that in this conformation, Thr83 from ecotin only occupies a small part of the S2 pocket, most of which is still left open to accommodate even larger hydrophobic residues. In its small molecule inhibitor bound state, Tyr^{H99} will likely deny Thr binding in the S2 pocket because of a clash between Thr83 and the O_η from Tyr^{H99}, which is less than 2 Å away.

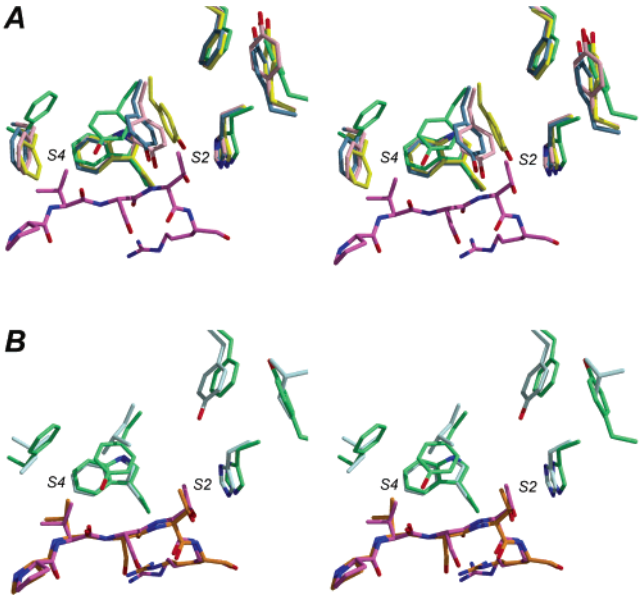

FIGURE 3: S2 and S4 substrate binding pockets of M84R−FXa (FXa−green, ecotin−purple) are shown superimposed in panel A with three FXa-inhibitor complexes (PDB 1XKA−yellow, 1EZQ−dark gray, and 1F0S−bright green) and in panel B with M84R−thrombin (PDB 1ID5; thrombin−white, ecotin−orange).

The S3 region, as is usual for serine proteases, is solvated. Aside from Gln at 192, no charged or other discriminatory residues are nearby. It has been hypothesized that the Gln at position 192 may contribute to FXa's preference for acidic residues at P3, as mutating Glu192 to Gln in both thrombin and activated protein C resulted in both enzymes selectively cleaving substrates with acidic residues at the P3 position (*37*, *38*). Our M84R−FXa structure indicates that a possible polar-charge interaction may occur between Gln^{H192} and the P3 residue (Figure 2A). The distances between the O_γ of Ser82 and the N_ϵ and O_ϵ of Gln^{H192} are 3.6 and 4.3 Å, respectively, and it is conceivable that in the presence of a negatively charged P3 residue, interactions could occur between the side chain of P3 and Gln^{H192}.

Together with two additional hydrophobic residues, Phe^{H174} and Trp^{H215}, residue Tyr^{H99} also defines the S4 substrate binding pocket (*7*) (Figures 2A and 3A). Its macromolecular inhibitor induced conformation inevitably changes the size of the S4 pocket. The long-established belief that the S4 pocket of FXa is fit to accommodate large bulky hydrophobic motifs no longer holds, as in M84R−FXa the S4 pocket shrinks to maximize interactions with a smaller residue such as Val. Although changes in the size of the S4 pocket are due in large part to Tyr^{H99}, Phe^{H174} also makes a significant contribution by rotating over 120° in response to Val81 from ecotin. The position of Trp^{H215} remains unchanged as the large flat floor of the S4 pocket (Figure 3A).

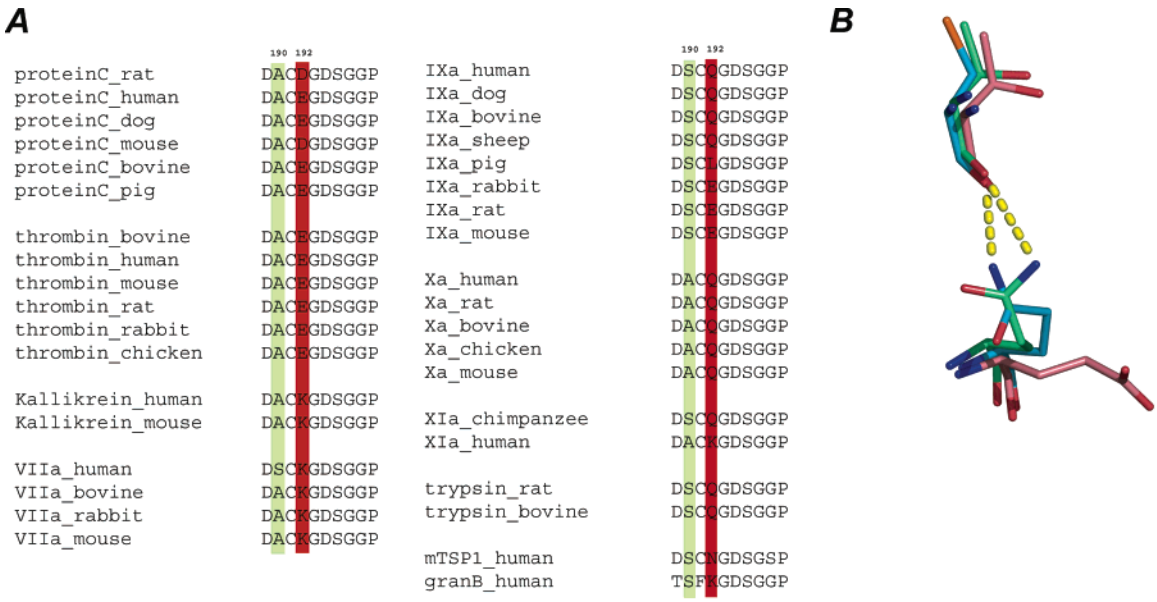

FIGURE 4: (A) Alignment of partial sequences of major serine proteases from the coagulation pathways. (B) Depicts the position of residue 192 and its interactions with the main-chain carbonyl of inhibitor P2 residue. M84R−FXa (green) is superimposed with two other structures, the M84R-thrombin (PDB 1ID5, pink) and thrombin E192Q-BPTI (PDB 1BTH, light blue).

Beyond P4, it is difficult to conclude whether there is any significant specificity. Our structure suggests that ecotin may bind FXa better if its Ser78 is replaced by a large charged residue to establish interactions with Ser^{H173}, Glu^{H217}, or Lys^{H224}. The primed site in FXa is also predominantly hydrophobic, but unlike thrombin the S1′ and S2′ pockets of FXa are well-separated by residue Gln^{H61}.

Residue 192 in Substrate and Inhibitor Discrimination. Besides its possible influence on acidic residues at the P3 position, residue 192 may have a more significant role in the regulation of coagulation proteases (*39*). Sequence alignments show that for the major serine proteases of the coagulation pathway, the amino acids surrounding the catalytic Ser^{H195} are almost completely conserved across species, with the exception of residues 192 and 190 (Figure 4A). In contrast to residue 190, which makes a fairly conservative fluctuation between Ala and Ser, residue 192 varies dramatically from the positively charged Lys (FVIIa), to the neutral but polar Gln (FXa) or Asn (mTSP), to the negatively charged Glu or Asp (thrombin and activated protein C (aPC)). In general, there is a trend in the charge of residue 192 from negative at the bottom of the coagulation cascade to positive at the top, which may be related to the order in which these enzymes evolved (*40*). Possibly because it served as an intermediate during the evolutionary process, FIXa is the only exception, showing a wide charge distribution among different species. Figure 2A,B reveals that 192 lies within hydrogen bonding distance to the P2 carbonyl oxygen of a substrate or canonically bound inhibitor (in this case, ecotin). The presence of a negatively charged residue at this position, as in thrombin and aPC (Figure 4A), would cause charge repulsion with any incoming P2 residue (Figure 4B). The energy barrier caused by such repulsion would not only render the protease more selective but also would decrease the likelihood of inhibition from such endogenous protease regulators such as tissue factor pathway inhibitor (TFPI) (*41*) and antithrombin III (ATIII) (*42*). This would explain why both human thrombin and aPC become highly susceptible to inhibition by bovine pancreatic trypsin inhibitor (BPTI) or TFPI once the negative charge at 192 is eliminated by mutagenesis (*38*, *43*, *44*). On the other hand, a positively charged or polar amine containing residue at 192 would be thought to have the opposite effect. In FXa, Gln^{H192} forms a hydrogen bond with the carbonyl oxygen of ecotin Ser83 (Figures 2B and 4B) promoting the proper alignment of interactions between ecotin and FXa. Together with residue Tyr^{H99}, it forms a clamp to secure tight binding of FXa to ecotin (Figure 2A).

While these results and others suggest a critical role for residue 192 in substrate and inhibitor discrimination, the role of other factors such as the presence of multiple extended surface loops and the conformation of subsite residues such as residue 99 must not be discounted (*45*). In addition, it is necessary to keep in mind that many of these studies were performed in vitro in the absence of a complete ensemble of physiological cofactors. While this does not detract from the relevance or utility of such studies toward a better understanding of these enzymes, in particular toward the design of more selective inhibitors, studies demonstrating the importance of exosite binding in the activity and regulation of these enzymes illustrate that a complete understanding of the coagulation proteases can only be achieved by considering the full context of these proteins in vivo (*46*−*50*).

Gla Domain—Overall Structure. In previous FXa structures, the Gla domain was either disordered or proteolytically cleaved to aid in crystallization (*2*, *5*, *7*−*9*, *19*). In the structure of M84R−FXa, all residues except the N-terminal three were ordered and unambiguously traced through electron density maps (Figure 5A). The Gla domain forms a bundle of three α helices that are stabilized by a core of hydrophobic amino acids composed of Leu^{L5}, Leu^{L13}, Tyr^{L24}, Ala^{L27}, Val^{L30}, Phe^{L31}, Phe^{L40}, Phe^{L41}, and Tyr^{L44} (Figure 5B). Except for Gla^{L39}, which is not involved in any contacts, all 11 Gla residues are involved in crystal contacts or Mg^{2+} binding and presumably would be solvent exposed in solution.

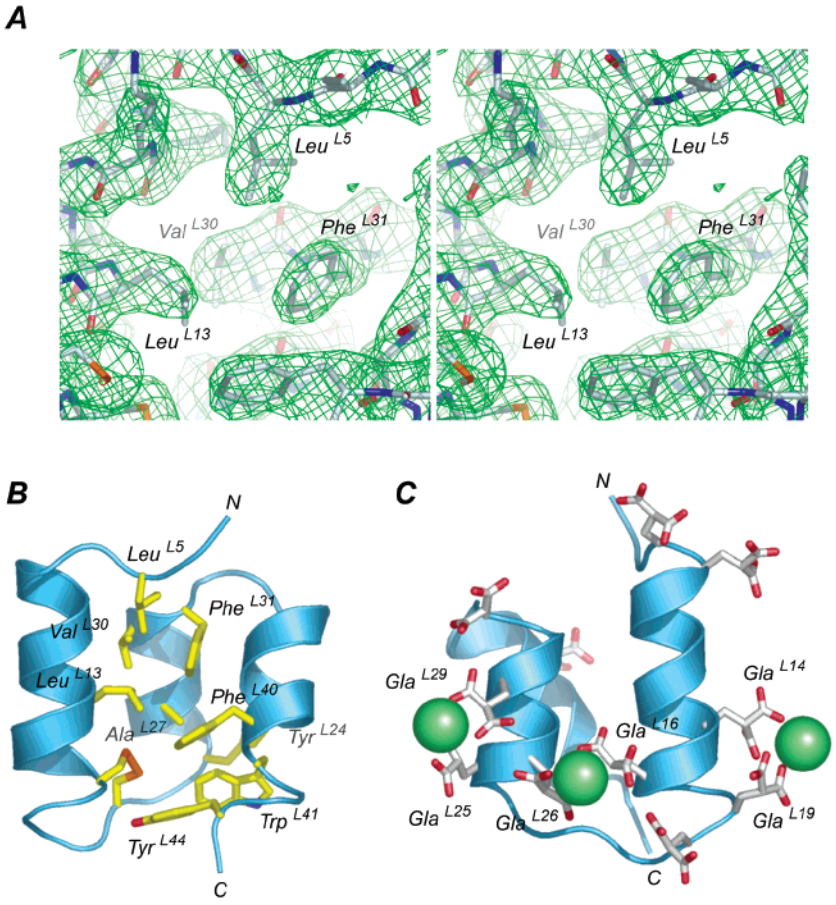

FIGURE 5: (A) Electron density of the Gla domain ($2F_{obs} - F_{calc}$) in the region around Leu^{L5} contoured at 1σ. (B and C) Two views of the Gla domain. Residues composing the hydrophobic core are highlighted in panel B while Gla residues and bound magnesium ions are shown in panel C.

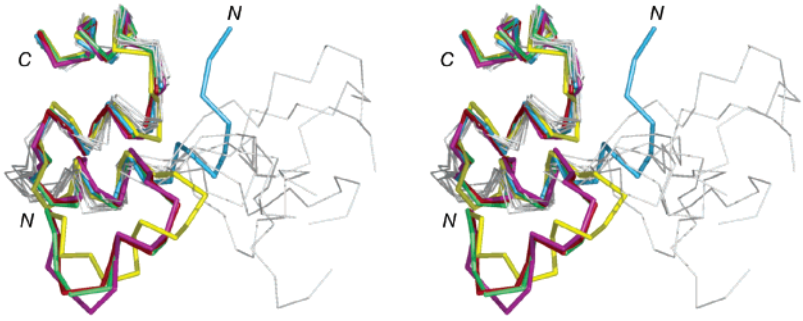

FIGURE 6: Gla domain of M84R−FXa (blue) superimposed with the calcium bound Gla domains of FVIIa (green), prothrombin (purple), FX (red), FIX (yellow), and the magnesium bound NMR structure of the FIX Gla domain (gray).

With the exception of the 11 N-terminal residues, the Gla domain of M84R−FXa is quite similar to structures reported for other Gla domains (Figure 6) (*51*−*55*). The rms deviations in the α carbon positions for residues 12−44 (FX numbering) between the M84R−FXa Gla domain and the Ca^{2+} bound structures of the prothrombin, FVIIa, FIX (lowest energy model), and the FX Gla domain are 0.72, 0.54, 0.87, and 0.56 Å, respectively. The rms deviation for the same residues of the lowest energy NMR structure with Mg^{2+} bound is 1.44 Å. Because of the unusual conformation of the N-terminus, the Gla domain of M84R−FXa forms a more globular structure than the flat, ellipsoid structures observed previously. The positions of the N-terminal 11 amino acids deviate quite dramatically from those previously observed. This Gla domain represents a novel conformation. In previous structures with Ca^{2+} bound, these residues form an ω loop structure whose Gla residues face toward the protein interior, and together with Gla residues from helix 1 and 2, chelate a line of Ca^{2+} ions. Three conserved hydrophobic residues at positions 4, 5, and 8, which are solvent exposed in this loop, are thought to be involved in interactions with the phospholipid membrane (*54*, *56*−*59*). In the one available structure with Mg^{2+} bound, the conformation of the N-terminal 11 residues are not defined because of disorder (*54*). These residues in M84R−FXa assume a largely helical structure, extending helix 1 by almost a full two turns as compared to the structures with Ca^{2+} bound. The remaining N-terminal residues (3−6) form a random coil partially extending over the top of the helical bundle. Leu^{L5} makes hydrophobic contacts with Phe^{L31}, effectively capping the top of the Gla domain's hydrophobic core (Figure 5A,B). The absence of the ω loop structure in the Gla domain of

M84R−FXa is probably due to the charge repulsion that would occur between Gla^{L6} and Gla^{L7} and Gla^{L16}, Gla^{L20}, Gla^{L26}, and Gla^{L29} upon formation of this structure in the presence of unoccupied Ca^{2+} binding sites.

Gla Domain−Mg^{2+} Binding. While the Gla domain can bind a number of different cations, only Ca^{2+} and Sr^{2+} have been shown to induce the state that binds phospholipid membranes (*20*). Previously, fluorescence, circular dichroism, and conformation-specific antibody studies on the homologous Gla domain of prothrombin have shown that there are two classes of cation binding sites (*20*−*23*). The first is composed of 3−4 cooperative, high affinity, but low specificity sites, while the second is characterized by 3−4 sites of lower affinity but higher specificity. Based on these observations, two cation-dependent folding transitions have been proposed (*23*). The first transition could be produced by binding to the nonspecific, high affinity sites, while the second transition responsible for the final membrane bound conformation may only be triggered by the specific binding of Ca^{2+} to the lower affinity sites.

Three large, positive difference electron density peaks between Gla^{L14} and Gla^{L19}, Gla^{L16} and Gla^{L26}, and Gla^{L25} and Gla^{L29} were modeled as Mg^{2+} ions because of the presence of 1 mM $MgCl_2$ in the crystallization buffer (Figure 5C). Previously, an NMR structure of the FIX Gla domain was solved in the presence of Mg^{2+}. However, because of cross-peak broadening, side chain positions were poorly defined, and the locations of the Mg^{2+} binding sites could not be deduced (*54*). Because of the presence of Mg^{2+} during crystallization and the finding that Mg^{2+} can induce the first transition but not the second (*20*), we believe that the locations of the three bound Mg^{2+} ions represent the three high affinity, low specificity sites predicted in earlier studies and that this structure represents an intermediate folding state of the Gla domain. At first glance, these sites would not be the ones predicted because they are spread out across the domain and do not appear to interact with each other. Indeed, the original sites proposed were adjacent to one another, and cooperativity was thought to be due to the orientation of Gla residues in a way that facilitated cation binding to an adjacent site in a polymeric array (*51*, *58*). Instead, we propose that the cooperativity observed in these high affinity sites is due more to global rearrangements of secondary and tertiary structure than to local rearrangements of side chains. In a scheme similar to that proposed previously (*54*), binding of a cation to one site would nucleate and stabilize secondary structure elements, organizing these elements into more ordered tertiary structure. This in turn would help properly position adjacent Gla residues for binding to the next site, which would then further order the domain and facilitate the positioning of Gla residues for cation binding at the last site. Binding at this last site would complete the transition to the intermediate state described here. Once in this intermediate state, we speculate that binding of Ca^{2+} to the remaining lower affinity sites promotes the ordering of the N-terminal residues into the ω loop structure and the formation of the final membrane bound state through bridging of Gla^{L6} and Gla^{L7} of the ω loop with Gla^{L16}, Gla^{L20}, Gla^{L26}, and Gla^{L29} via bound Ca^{2+} ions.

This model is supported by NMR and crystal structures of the Gla domain solved in the absence of Ca^{2+} (*52*, *58*, *60*). In these structures, the Gla domain has clearly defined elements of secondary structure, but individual helices are truncated and do not form well-ordered tertiary structure. Moreover, the NMR structure of the FIX Gla domain in the presence of Mg^{2+} shows that while most of the Gla domain is well-ordered, forming a globular core essentially equivalent to that seen in the Ca^{2+} bound structures, residues 1−11 have no defined structure (Figure 6) (*54*). In addition, equilibrium dialysis studies have shown that in the presence of Mg^{2+}, Ca^{2+} affinity is increased (*21*). This observation, combined with studies that have shown that Mg^{2+} can promote the first transition but not the second required for phospholipid binding (*20*), suggests that binding to the high affinity sites primes the Gla domain for Ca^{2+} binding at the low affinity sites and subsequent formation of the membrane bound conformation. Although the possibility exists that the unusual conformation of the N-terminal 11 residues observed here does not exist in solution, and may have been induced by crystal contacts, the finding in NMR studies that these residues are disordered in the absence of Ca^{2+} implies that the N-terminus is highly flexible and may attain a number of different conformations. The capping of the hydrophobic core of the domain by Leu^{L5} and the formation of additional secondary structure through the N-terminal extension of helix 1, both energetically favorable interactions, suggest that this conformation is not a mere crystallization artifact, and we speculate as to whether this may indeed be biologically relevant. Further experiments will show whether this is the case.

ACKNOWLEDGMENT

The authors would like to thank Haematologic Technologies Inc. for their assistance in the purification of the factor Xa-ecotin M84R complex.

REFERENCES

1. Davie, E. W., Fujikawa, K., and Kisiel, W. (1991) The coagulation cascade: initiation, maintenance, and regulation, *Biochemistry 30* (43), 10363−70.
2. Padmanabhan, K., et al. (1993) Structure of human des(1−45) factor Xa at 2.2 Å resolution, *J. Mol. Biol. 232* (3), 947−66.
3. Kaiser, B. (2002) Factor Xa−a promising target for drug development, *Cell Mol. Life Sci. 59* (2), 189−92.
4. Stubbs, M. T., and Bode, W. (1994) Coagulation factors and their inhibitors, *Curr. Opin. Struct. Biol. 4* (6), 823−32.
5. Brandstetter, H., et al. (1996) X-ray structure of active site-inhibited clotting factor Xa. Implications for drug design and substrate recognition, *J. Biol. Chem. 271* (47), 29988−92.
6. Wei, A., et al. (1998) Unexpected binding mode of tick anticoagulant peptide complexed to bovine factor Xa, *J. Mol. Biol. 283* (1), 147−54.
7. Kamata, K., et al. (1998) Structural basis for chemical inhibition of human blood coagulation factor Xa, *Proc. Natl. Acad. Sci. U.S.A. 95* (12), 6630−5.
8. Adler, M., et al. (2000) Preparation, characterization, and the crystal structure of the inhibitor ZK-807834 (CI-1031) complexed with factor Xa, *Biochemistry 39* (41), 12534−42.
9. Maignan, S., et al. (2000) Crystal structures of human factor Xa complexed with potent inhibitors, *J. Med. Chem. 43* (17), 3226−32.
10. Rezaie, A. R., and Yang, L. (2001) Probing the molecular basis of factor Xa specificity by mutagenesis of the serpin, antithrombin, *Biochim. Biophys. Acta 1528* (2−3), 167−76.
11. Chung, C. H., et al. (1983) Purification from *Escherichia coli* of a periplasmic protein that is a potent inhibitor of pancreatic proteases, *J. Biol. Chem. 258* (18), 11032−8.
12. Seymour, J. L., et al. (1994) Ecotin is a potent anticoagulant and reversible tight-binding inhibitor of factor Xa, *Biochemistry 33* (13), 3949−58.

13. Ulmer, J. S., et al. (1995) Ecotin is a potent inhibitor of the contact system proteases factor XIIa and plasma kallikrein, *FEBS Lett. 365* (2−3), 159−63.
14. McGrath, M. E., et al. (1994) Macromolecular chelation as an improved mechanism of protease inhibition: structure of the ecotin−trypsin complex, *EMBO J. 13* (7), 1502−7.
15. Perona, J. J., et al. (1997) Crystal structure of an ecotin−collagenase complex suggests a model for recognition and cleavage of the collagen triple helix, *Biochemistry 36* (18), 5381−92.
16. Waugh, S. M., et al. (2000) The structure of the pro-apoptotic protease granzyme B reveals the molecular determinants of its specificity, *Nat. Struct. Biol. 7* (9), 762−5.
17. Wang, S. X., Esmon, C. T., and Fletterick, R. J. (2001) Crystal structure of thrombin-ecotin reveals conformational changes and extended interactions, *Biochemistry 40* (34), 10038−46.
18. Furie, B., and Furie, B. C. (1988) The molecular basis of blood coagulation, *Cell 53* (4), 505−18.
19. Nar, H., et al. (2001) Structural basis for inhibition promiscuity of dual specific thrombin and factor Xa blood coagulation inhibitors, *Structure* (*Cambridge*) *9* (1), 29−37.
20. Nelsestuen, G. L., Broderius, M., and Martin, G. (1976) Role of γ-carboxyglutamic acid. Cation specificity of prothrombin and factor X-phospholipid binding, *J. Biol. Chem. 251* (22), 6886−93.
21. Prendergast, F. G., and Mann, K. G. (1977) Differentiation of metal ion-induced transitions of prothrombin fragment 1, *J. Biol. Chem. 252* (3), 840−50.
22. Bloom, J. W., and Mann, K. G. (1978) Metal ion induced conformational transitions of prothrombin and prothrombin fragment 1, *Biochemistry 17* (21), 4430−8.
23. Borowski, M., et al. (1986) Prothrombin requires two sequential metal-dependent conformational transitions to bind phospholipid. Conformation-specific antibodies directed against the phospholipid-binding site on prothrombin, *J. Biol. Chem. 261* (32), 14969−75.
24. McGrath, M. E., et al. (1991) Expression of the protease inhibitor ecotin and its cocrystallization with trypsin, *J. Mol. Biol. 222* (2), 139−42.
25. Yang, S. Q., et al. (1998) Ecotin: a serine protease inhibitor with two distinct and interacting binding sites, *J. Mol. Biol. 279* (4), 945−57.
26. Otwinowski, Z., and Minor, W. (1997) *Methods in Enzymology* (Carter, C. W. and Sweet, R. M., Eds.) p 307−26, Academic Press, New York.
27. Brunger, A. T., et al. (1998) Crystallography and NMR system: A new software suite for macromolecular structure determination, *Acta Crystallogr. D4* (Pt 5), 905−21.
28. Hubbard, S. J., and Thornton, J. M. (1993) *Naccess, computer program.* Department of Biochemistry and Molecular Biology, University of College London.
29. Kleywegt, G. J. (1996) Use of noncrystallographic symmetry in protein structure refinement, *Acta Crystallogr. D52*, 842−57.
30. Browner, M. F., Fauman, E. B., and Fletterick, R. J. (1992) Tracking conformational states in allosteric transitions of phosphorylase, *Biochemistry 31* (46), 11297−304.
31. Merritt, E. A., and Bacon, D. J. (1997) Raster3D: Photorealistic Molecular Graphics, *Methods Enzymol. 277*, 505−24.
32. Wallace, A. C., Laskowski, R. A., and Thornton, J. M. (1995) LIGPLOT: a program to generate schematic diagrams of protein−ligand interactions, *Protein Eng. 8* (2), 127−34.
33. DeLano, W. L. (2002) *The PyMOL Molecular Graphics System*, DeLano Scientific, San Carlos, CA.
34. Schechter, I., and Berger, A. (1967) On the size of the active site in proteases. I. Papain, *Biochem. Biophys. Res. Commun. 27* (2), 157−62.
35. Harris, J. L., et al. (2000) Rapid and general profiling of protease specificity by using combinatorial fluorogenic substrate libraries, *Proc. Natl. Acad. Sci. U.S.A. 97* (14), 7754−9.
36. Bianchini, E. P., et al. (2002) Mapping of the catalytic groove preferences of factor xa reveals an inadequate selectivity for its macromolecule substrates, *J. Biol. Chem. 277* (23), 20527−34.
37. Le Bonniec, B. F., and Esmon, C. T. (1991) Glu-192−Gln substitution in thrombin mimics the catalytic switch induced by thrombomodulin, *Proc. Natl. Acad. Sci. U.S.A. 88* (16), 7371−5.
38. Rezaie, A. R., and Esmon, C. T. (1993) Conversion of glutamic acid 192 to glutamine in activated protein C changes the substrate specificity and increases reactivity toward macromolecular inhibitors, *J. Biol. Chem. 268* (27), 19943−8.
39. Rezaie, A. R., and Esmon, C. T. (1995) Contribution of residue 192 in factor Xa to enzyme specificity and function, *J. Biol. Chem. 270* (27), 16176−81.
40. Krem, M. M., and Cera, E. D. (2002) Evolution of enzyme cascades from embryonic development to blood coagulation, *Trends Biochem. Sci. 27* (2), 67−74.
41. Broze, G. J., Jr., Girard, T. J., and Novotny, W. F. (1990) Regulation of coagulation by a multivalent Kunitz-type inhibitor, *Biochemistry 29* (33), 7539−46.
42. Kisiel, W. (1979) Molecular properties of the Factor V-activating enzyme from Russell's viper venom, *J. Biol. Chem. 254* (23), 12230−4.
43. Guinto, E. R., et al. (1994) Glu192 → Gln substitution in thrombin yields an enzyme that is effectively inhibited by bovine pancreatic trypsin inhibitor and tissue factor pathway inhibitor, *J. Biol. Chem. 269* (28), 18395−400.
44. van de Locht, A., et al. (1997) The thrombin E192Q−BPTI complex reveals gross structural rearrangements: implications for the interaction with antithrombin and thrombomodulin, *EMBO J. 16* (11), 2977−84.
45. Rezaie, A. R. (1996) Role of residue 99 at the S2 subsite of factor Xa and activated protein C in enzyme specificity, *J. Biol. Chem. 271* (39), 23807−14.
46. Vijayalakshmi, J., et al. (1994) The isomorphous structures of prethrombin2, hirugen-, and PPACK-thrombin: changes accompanying activation and exosite binding to thrombin, *Protein Sci. 3* (12), 2254−71.
47. Rezaie, A. R. (2000) Heparin-binding exosite of factor Xa, *Trends Cardiovasc. Med. 10* (8), 333−8.
48. Dennis, M. S., et al. (2000) Peptide exosite inhibitors of factor VIIa as anticoagulants, *Nature 404* (6777), 465−70.
49. Fuentes-Prior, P., et al. (2000) Structural basis for the anticoagulant activity of the thrombin-thrombomodulin complex, *Nature 404* (6777), 518−25.
50. Chuang, Y. J., et al. (2001) Heparin enhances the specificity of antithrombin for thrombin and factor Xa independent of the reactive center loop sequence. Evidence for an exosite determinant of factor Xa specificity in heparin-activated antithrombin, *J. Biol. Chem. 276* (18), 14961−71.
51. Soriano-Garcia, M., et al. The Ca^{2+} ion and membrane binding structure of the Gla domain of Ca-prothrombin fragment 1, *Biochemistry 31* (9), 2554−66.
52. Freedman, S. J., et al. (1995) Structure of the calcium ion-bound γ-carboxyglutamic acid-rich domain of factor IX, *Biochemistry 34* (38), 12126−37.
53. Banner, D. W., et al. (1996) The crystal structure of the complex of blood coagulation factor VIIa with soluble tissue factor, *Nature 380* (6569), 41−6.
54. Freedman, S. J., et al. (1996) Identification of the phospholipid binding site in the vitamin K-dependent blood coagulation protein factor IX, *J. Biol. Chem. 271* (27), 16227−36.
55. Mizuno, H., et al. (2001) Crystal structure of an anticoagulant protein in complex with the Gla domain of factor X, *Proc. Natl. Acad. Sci. U.S.A. 98* (13), 7230−4.
56. Zhang, L., and Castellino, F. J. (1994) The binding energy of human coagulation protein C to acidic phospholipid vesicles contains a major contribution from leucine 5 in the γ-carboxyglutamic acid domain, *J. Biol. Chem. 269* (5), 3590−5.
57. Christiansen, W. T., et al. (1995) Hydrophobic amino acid residues of human anticoagulation protein C that contribute to its functional binding to phospholipid Vesicles, *Biochemistry 34* (33), 10376−82.
58. Sunnerhagen, M., et al. (1995) Structure of the Ca^{2+}-free Gla domain sheds light on membrane binding of blood coagulation proteins, *Nat. Struct. Biol. 2* (6), 504−9.
59. Falls, L. A., et al. (2001) The ω-loop region of the human prothrombin γ-carboxyglutamic acid domain penetrates anionic phospholipid membranes, *J. Biol. Chem. 276* (26), 23895−902.
60. Tulinsky, A., Park, C. H., and Skrzypczak-Jankun, E. (1988) Structure of prothrombin fragment 1 refined at 2.8 Å resolution, *J. Mol. Biol. 202* (4), 885−901.
61. Kleywegt, G. J., and Brunger, A. T. (1996) Checking your imagination: applications of the free *R* value, *Structure 4* (8), 897−904.

BI027320A